Nuclear Engineering and Technology 50 (2018) 907–914

Contents lists available at ScienceDirect

Nuclear Engineering and Technology

journal homepage: www.elsevier.com/locate/net

Original Article

Molecular dynamics simulations of the coupled effects of strain and temperature on displacement cascades in α-zirconium

Qurat-ul-ain Sahi, Yong-Soo Kim*

Department of Nuclear Engineering, Hanyang University, 222 Wangsimni-ro, Seongdong-gu, Seoul, 133-791, Republic of Korea

ARTICLE INFO

Article history:
Received 26 January 2018
Received in revised form
16 March 2018
Accepted 16 April 2018
Available online 23 April 2018

Keywords:
Defect Clusters
Displacement Cascade
Molecular Dynamics
Primary Defect Formation
Strain Effects
Temperature Effects

ABSTRACT

In this article, we conducted molecular dynamics simulations to investigate the effect of applied strain and temperature on irradiation-induced damage in alpha-zirconium. Cascade simulations were performed with primary knock-on atom energies ranging between 1 and 20 KeV, hydrostatic and uniaxial strain values ranging from −2% (compression) to 2% (tensile), and temperatures ranging from 100 to 1000 K. Results demonstrated that the number of defects increased when the displacement cascade proceeded under tensile uniaxial hydrostatic strain. In contrast, compressive strain states tended to decrease the defect production rate as compared with the reference no-strain condition. The proportions of vacancy and interstitial clustering increased by approximately 45% and 55% and 25% and 32% for 2% hydrostatic and uniaxial strain systems, respectively, as compared with the unstrained system, whereas both strain fields resulted in a 15–30% decrease in vacancy and interstitial clustering under compressive conditions. Tensile strains, specifically hydrostatic strain, tended to produce larger sized vacancy and interstitial clusters, whereas compressive strain systems did not significantly affect the size of defect clusters as compared with the reference no-strain condition. The influence of the strain system on radiation damage became more significant at lower temperatures because of less annealing than in higher temperature systems.

1. Introduction

The interactions of energetic ions with solids in structural materials result in defect production, cluster formation, and colloid interactions. In irradiation environments, highly energetic ions impart their energy to the target material, which leads to localized defect production in the form of vacancies, interstitials, and substitutional voids within the lattice, altering the microstructural properties of the target material as well as its mechanical and physical properties [1,2]. Defect generation by irradiation can also result in microscopic and macroscopic deformation of the target material. Changes in the physical properties of materials under irradiation depend on the concentration and mobility of defects. The production of these defects, in turn, is determined by irradiation parameters such as the energy and type of incident ions, temperature, and strains applied to the materials during irradiation [3].

Zirconium (Zr) and its alloys are important in the nuclear power plant industry because of their widespread use in reactor core structural materials such as pressure water tubes, calendric tubes, and fuel cladding. Core structural materials are exposed to harsh irradiation, temperatures, and stress/strain environments during reactor operation [4]. High-energy neutrons produce surface hardening, phase stability, irradiation growth, and precipitation inside Zr and its alloys. Alpha (α)-Zr with a hexagonal closed-pack structure has a low thermal neutron absorption cross section, high corrosion resistance, and good mechanical properties [5]. Several experimental studies have examined the effects of irradiation on the microstructure of Zr and its alloys [5–7]. Such experimental approaches have examined the microstructure and mechanical properties of the materials in detail, but information about the primary defect generation and propagation of defects in the materials has not been generated.

The interaction of energetic ions with the material produces displacement cascades and clustering of both vacancies and interstitials. Knowledge of radiation damage at smaller timescale (1–2 ps) using molecular dynamics (MD) simulations is crucial for successful prediction and assessment of material performance in

* *Corresponding author.*
E-mail addresses: quratsahi@hanyang.ac.kr (Q.-u.-a. Sahi), yongskim@hanyang.ac.kr (Y.-S. Kim).

https://doi.org/10.1016/j.net.2018.04.013

reactor power systems [8]. Previous MD simulation studies [9–11] of Zr were conducted mainly by using the embedded-atom method (EAM) potential developed by Ackland et al. [12], which is known to have the limitation of calculating stacking fault energies using *ab initio* calculations [13,14]. Although continuous efforts have been made to examine the effects of energy on primary radiation damage and the mobility of defects, very few studies consider the potential effects of strain and temperature on radiation damage–induced defects in α-Zr [9–11]. However, the irradiation-induced swelling, void swelling, solute segregation, and alloying/solute precipitates can generate strain fields (up to 5% in one crystallography direction) due to the associated local volume expansion [15]. A previous study [16] reported the effects of uniaxial strain (up to 1% compression/tension) for 10-KeV primary-knock on atom (PKA) energy in pure Zr along the [10–10] and [0002] crystallographic directions, wherein the authors found that the strains up to 1% influenced the size of vacancy/interstitial clusters to a greater extent than the total number of Frenkel pairs generated and the number of vacancy/interstitial clusters. They investigated the effect of strain on Zr at 100 K; however, the temperature inside a nuclear reactor core is usually much higher than this. It is noteworthy to mention that the previous modeling endeavors focused on the effect of energy and temperature independently [9,11,16], but to the best of our knowledge, coupling effects of strain and temperature have not yet been explored for α-Zr.

Therefore, in this article, we used MD simulations to investigate the coupled effects of two different applied (hydrostatic and uniaxial) strain fields and lattice temperatures varying from 100 to 1000 K on generation of primary radiation damage in α-Zr provided with PKA energies of 1–20 KeV. Simulations are described in detail in the next section, followed by presentation of our results regarding the production of point defects (i.e., vacancies and interstitials), their behavior, evolution, and aggregation into vacancy and interstitial clusters under different strain and temperatures. Finally, the mechanisms underlying the obtained results are discussed in Section 4.

2. Simulation methods

All displacement cascade simulations discussed here were carried out using the classical molecular dynamics software package LAMMPS (Large-scale Atomic/Molecular Massively Parallel Simulator) developed and maintained by Sandia National Laboratories [17]. We described the interatomic interaction between Zr atoms by the EAM interatomic potential modified by Mendelev and Ackland [18] in 2007 named Zr #3. Previous studies [13,14] have shown that Mendelev EAM potential provides the best fitting of defect properties to *ab initio* calculations [19,20]. Atomic interactions were smoothly fitted with universal Ziegler–Biersack–Littmarks potentials [21] for short-range interactions (active at only very short-–range distances). Before initial displacement damage simulations, all hexagonal closed-pack simulation cells of Zr atoms were allowed to thermally equilibrate for 50 ps at 300 K in an NPT (constant atoms, pressure, and temperature) ensemble. Periodic boundary conditions were applied in all three directions. Then uniaxial strain along the c-axis ([0001]) and hydrostatic strain ranging between −2% and 2% were applied, and the strained lattice was allowed to relax for an extra 30 ps in a canonical NVT (constant atom, constant volume, and constant temperature) ensemble. Negative values for both strain types correspond to compression deformation, whereas positive values correspond to tensile deformation. For hydrostatic strain type, the same strain values were applied along all axes of the simulation cell as this strain type has a uniform volumetric strain field. After the simulation cell reached the preset strain value, the current sizes were kept for further displacement cascade simulations.

The displacement cascade was initiated by providing the required amount of kinetic energy in the form of instantaneous velocity to a selected PKA near the center of the simulation cell. Because the PKA recoil direction does not have any significant influence on damage generation and final surviving damage stage, we have chosen a high-indexed crystallographic direction [2 31 9] to avoid channeling [11,22,23]. Energies of the displacement cascade were 1, 5, 10, and 20 KeV for each strain type and strain value. As the combination of each strain and PKA energy may affect the results, three different sizes of simulation cells containing Zr atoms were constructed to avoid the displacement cascade interfering with the boundaries. For all PKA energies, radiation-induced displacement cascades were allowed to evolve and relax for several picoseconds with a timestep of 0.2 fs until the temperature of the displacement cascade core and the generated number of defect displacements reached a stable state. It is important to note that all cascade simulations were carried out in an NVE (constant atoms, constant volume, and constant energy) ensemble. Theoretically, the standard number of atomic displacements can also be numerically estimated by the Norgott–Robinson–Torrens method using the following equation:

$$\nu_{NRT} = \frac{0.8E_{PKA}}{2E_d} \quad (1)$$

where E_d is the value of threshold displacement energy of the material, which here, for Zr, is chosen to be 40 eV according to the international American Society for Materials and Testing standards [24]. The detailed parameters of the simulation and standard Norgott–Robinson–Torrens displacements are summarized in Table 1. To investigate the coupling effect of the applied strain and temperature, various simulations were performed at five different temperatures (100 K, 300 K, 600 K, 1000 K, and 1200 K) for each strain type and value, with 20-KeV PKA energy. The sizes of simulation cells were also increased with an increase in lattice temperature to avoid heating up of the system and displacement of the cascade core.

The Wigner–Sitz (W–S) cell method was used to analyze the atomic configurations in the simulation cell during the displacement cascade and at the end of simulation cascade by using the processing and visualization software OVITO. OVITO is a freely available software which is developed by Alexander Stukowski at Darmstadt University of Technology, Germany. An empty W-S cell with no Zr atoms corresponds to a vacancy, whereas a W-S cell with two Zr atoms is identified as interstitial. The defect cluster states were analyzed by the nearest neighbor criterion; for vacancy and interstitial clusters, the most commonly used cutoff radii of first and second nearest neighbor distances were used, respectively [25].

3. Results

The effects of applied strain fields on defect (vacancies and interstitials) yield and their clustering were averaged over eight independent MD simulations carried out with various random PKA positions to obtain statistically meaningful results. It is noted that error bars included in the figures denote the standard error of the

Table 1
Typical parameters of MD cascade simulations and calculated NRT displacements.

PKA energy (KeV)	No of simulations	NRT displacements	Atoms in simulation	Simulation time (ps)
1	8	10	80640	10
5	8	50	250880	10
10	8	100	250880	20
20	8	200	348192	20

MD, molecular dynamics; NRT, Norgott–Robinson–Torrens; PKA, primary knock-on atom.

mean of dataset for each case. Because each strain type and value showed a similar thermal spike and lifetime for all given PKA energies, the typical response to 20-KeV PKA energy with time is shown in Fig. 1 as a representative example, which illustrates the impact of strain on the peak and surviving number of defects with time evolution. The data points in Fig. 1 are shifted to left side by 1.3 units. For tensile strains, the peak started a bit earlier and attained a larger height and also lasted longer, whereas for compression, the peak started relatively later than the reference condition with no strain. Therefore, to gain more insight into the effects of PKA energy and strain type, we compared the generated number of defects at each PKA energy and strain value.

3.1. PKA energy effects

When analyzing radiation damage, the energy of the incident ion should be taken into account as neutrons in the reactor may have energies in the range of tens of MeV and can transfer hundreds of KeV of energy to PKAs. To adequately simulate such higher energies, simulation system should have at least 20 millions of atoms which may also have many other limitations along with the computation system. However, delivery of 10-KeV energy to the PKA can produce well-defined subcascades; we therefore limited our simulations to 20-KeV PKA energy [26]. The dependence of the surviving number of Frenkel pairs for unstrained and 2% uniaxial and hydrostatic strain systems as a function of PKA energy is presented in Fig. 2. Dependence was not linear but followed an empirical power law [27] $N_{FP} = A(E_{PKA})^b$, with A = 3.81, 6.98, and 8.10 and b = 0.65, 0.52, and 0.66 for unstrained, 2% uniaxial, and 2% hydrostatic strained systems, respectively. The surviving number of Frenkel pairs (vacancy–interstitial pairs) increased gradually with an increase in the PKA energy. This is because the initially created PKA produced a subsequent chain of atomic displacement events in the sample material as soon as energy was provided to the PKA. The energy of the PKA was then transferred to many other atoms of the sample material during multiple atomic interactions, and these collisional events continued until the energy transferred to the PKA was distributed over the entire volume of the simulation cell and no atom had energy greater than the threshold displacement energy of that material [1]. At higher PKA energies, the energy dependence was more linear because of the high energy of secondary knock-on atoms, which behaved as displacement cascades of lower energy than the initial PKA energy. For hydrostatic strained systems, the dependence of the surviving number of defects increased in a linear manner. This could be due to increased generation of atomic defects during a longer thermal spike and the increase in size of the cascade-damage core with simulation time (Fig. 1) as compared with the reference condition with no applied strain.

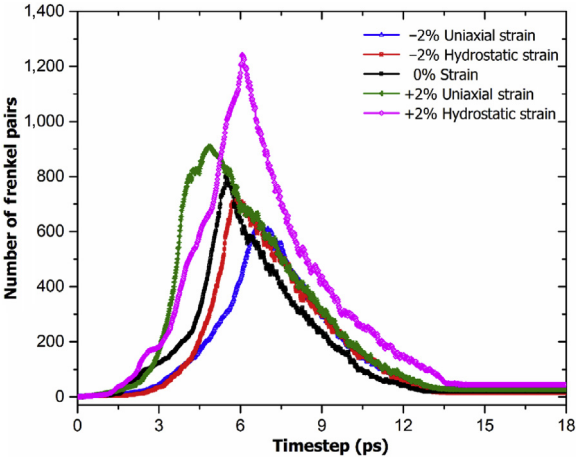

Fig. 1. Time evolution of defects produced during displacement cascade of 20 KeV for various applied strain values.

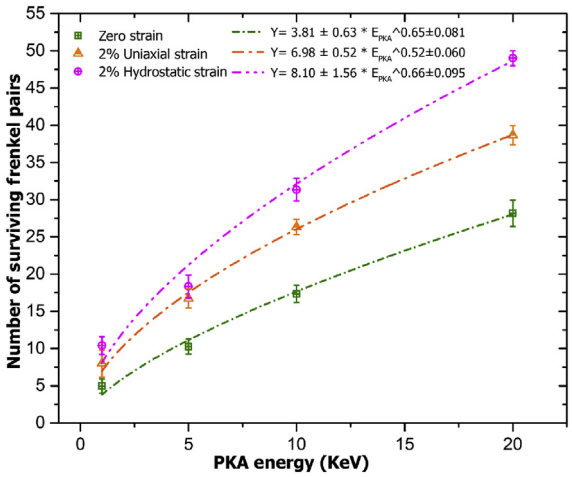

Fig. 2. Surviving number of Frenkel pairs as a function of PKA energy for unstrained and strained systems.
PKA, primary knock-on atom.

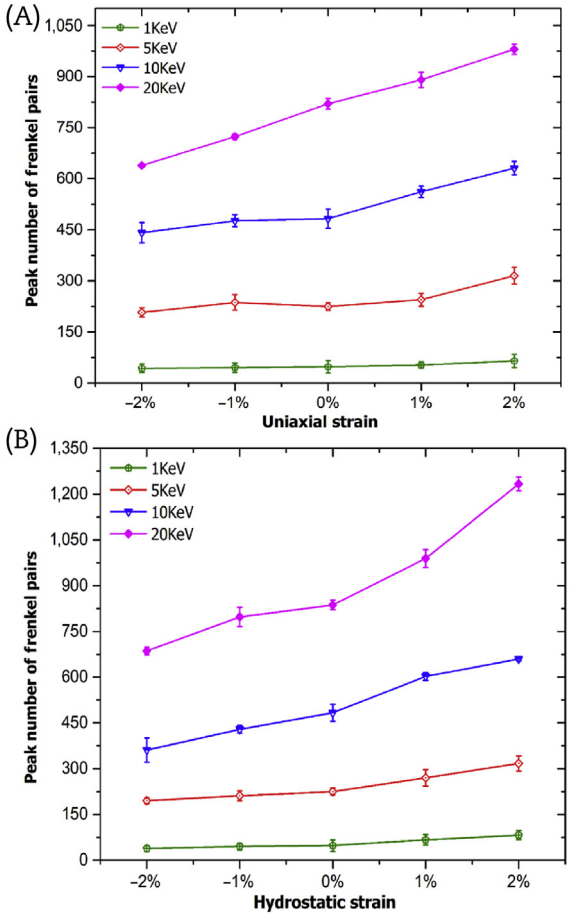

Fig. 3. Estimated peak number of Frenkel pairs for various PKA energies. (A) As a function of applied uniaxial strain. (B) As a function of hydrostatic strain.
PKA, primary knock-on atom.

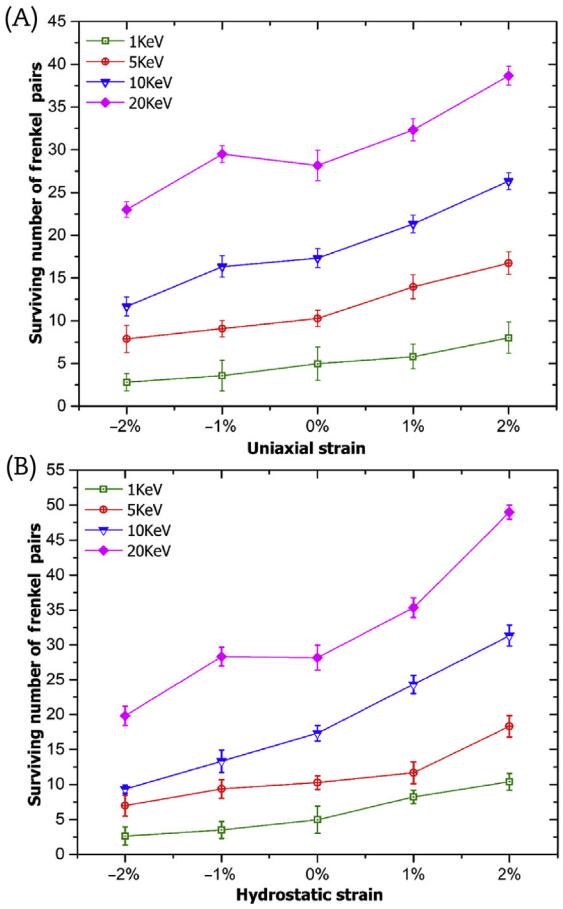

Fig. 4. Number of surviving Frenkel pairs for various PKA energies. (A) As a function of applied uniaxial strain (B) As a function of applied hydrostatic strain.
PKA, primary knock-on atom.

3.2. Strain effects

3.2.1. Point defects

The effects of strain type and strain values on defect generation were also investigated for different PKA energies. Collision cascades have three distinctive stages: During the initial picoseconds of displacement cascade initiation, there is a so-called ballistic phase that takes place as soon as energy is transferred to the PKA and a large number of atoms being displaced from their original lattice site. Following the ballistic stage (0.1–0.5 ps) is a thermal spike where extremely spatial inhomogeneity of pressure, density, and temperature is generated in some cases. Most of the atoms displaced during the earlier stages return to the regular crystal lattice sites during the successive picoseconds (annealing/relaxation). At the end of the cascade, only a reduced fraction of defects and defect clusters survive through the relaxation stage. The main features of the ballistic stage are the peak (maximum) number of atomic displacements and the corresponding peak time (the time interval between initiation of the cascade and when the largest number of defects is produced). The peak number of atomic defects as a function of strain type and values for all PKA energies is presented in Fig. 3. These results show that the peak number of defects tended to increase with positive (tensile) strain for both uniaxial and hydrostatic strain fields as compared with the reference condition with no strain. This increase was most noticeable for 20-KeV PKA energy under positive strain conditions. Furthermore, under larger positive strains, the larger the positive volume change is, the greater the number of defects created and vice versa.

The number of surviving Frenkel pairs (vacancy–interstitial pairs) after cooldown of the damage cascade core is an important parameter to consider when estimating radiation damage and investigating the mobility of defects and their aggregation into clusters. Fig. 4 shows the final number of Frenkel pairs for each combination of PKA energy and strain. There was significant variation in the number of Frenkel pairs for both strains types; however, these variations were more prominent for the hydrostatic strain system. The positive (tensile) tensile strain state for both uniaxial and hydrostatic strain increased the number of defects as compared with the reference condition with no strain. In contrast, negative (compression) strain states reduced the number of surviving defects. When hydrostatic strain was applied with PKA energy of 20 KeV, the increase in number of defects was much larger for the tension condition than for the reference condition with no applied strain. Therefore, under hydrostatic strain, the larger the tension strain, the greater the number of surviving defects and vice versa. This increase/decrease in number of produced or surviving Frenkel pairs with tension/compression suggests that the applied strain influences the cascade process by affecting the energetics of formation and recombination of Frenkel pairs [28,29]. Overall, the larger the degree of applied tensile strain, the lower the energy of the atoms that cause damage. Thus, tensile stress/strain conditions should be avoided for materials exposed to irradiation.

Defect production efficiency versus PKA energy for unstrained and strain systems is shown in Fig. 5. It is well known from previous studies that the number of surviving Frenkel pairs increases with increasing PKA energy, but at a decreasing rate, the efficiency of defect production during cascade damage process decreases as

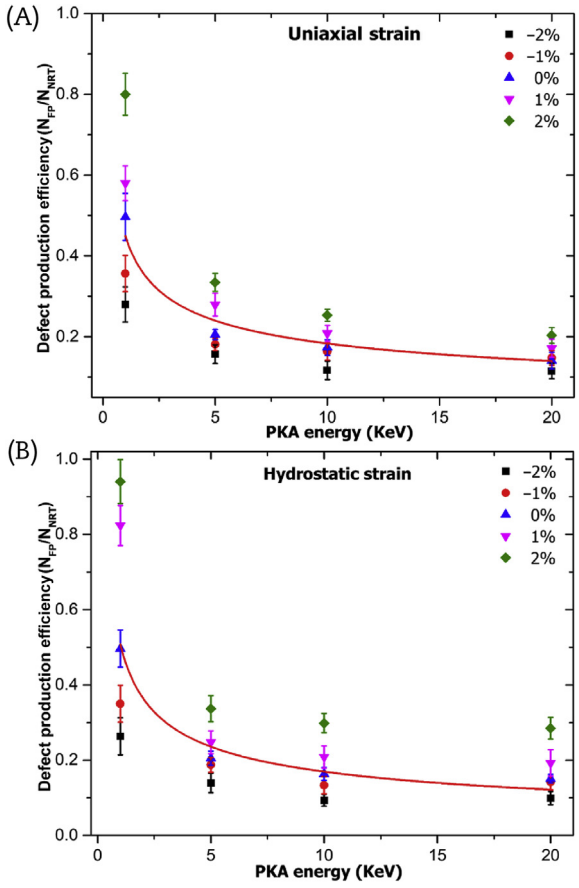

Fig. 5. Defect production efficiency as a function of PKA energy. (A) For uniaxial strain. (B) For hydrostatic strain.
PKA, primary knock-on atom.

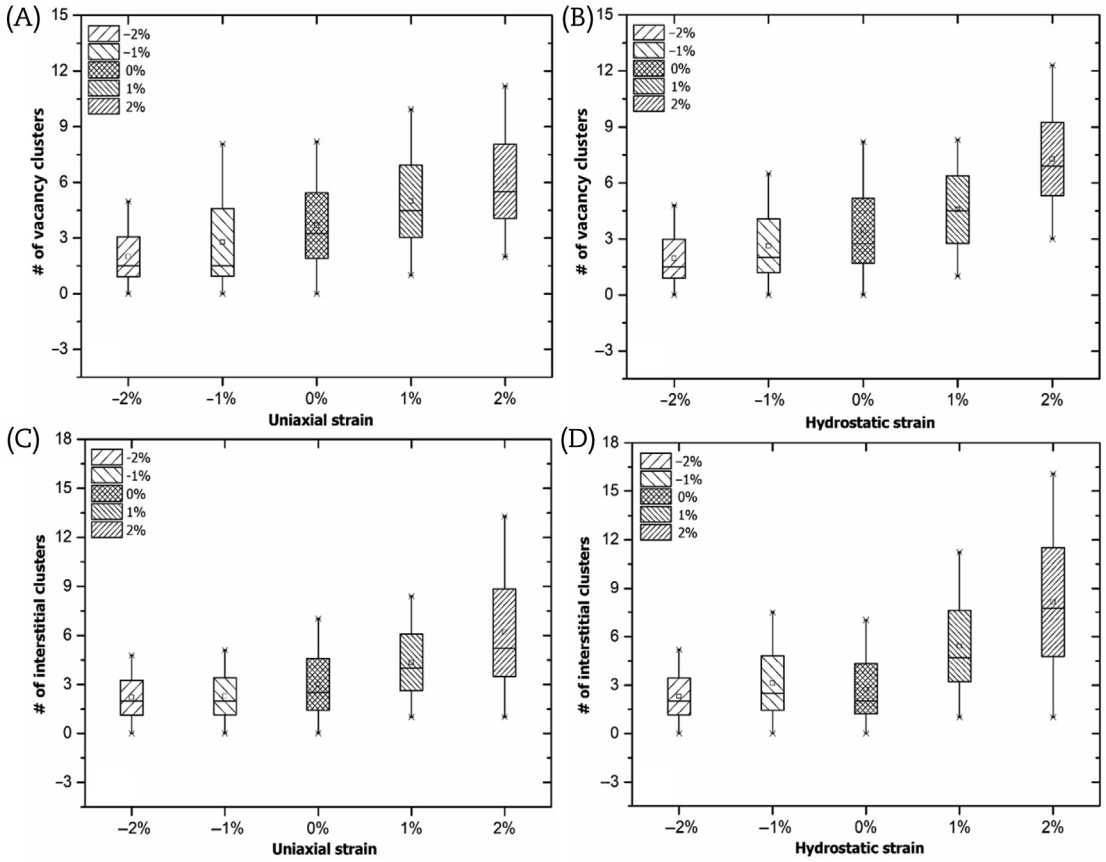

Fig. 6. Vacancies and interstitials clustering for various PKA energies. (A & C) As a function of uniaxial strain. (B & D) As a function of hydrostatic strain. PKA, primary knock-on atom.

the PKA energy increases. Our results demonstrate that defect production efficiency behavior was similar for no strain, uniaxial, and hydrostatic strain conditions. For the uniaxial system, with or without strain, defect production efficiency decreased gradually until 20 KeV, whereas positive (tensile) hydrostatic strain showed almost stable efficiency of defect production for energies of 10 and 20 KeV.

3.2.2. Defect clusters and size distribution

The tendency of point defects to agglomerate into clusters may aggravate radiation damage because the characteristics of clusters influence the form and temperature/strain dependence of damage accumulation as the microstructure evolves. Fig. 6 shows the number of vacancy and interstitial clusters for each combination of energy and strain type in the form of box plots, where each box presents the number of vacancy/interstitial clusters for the range of PKA energies for the corresponding strain type and strain value. For both uniaxial and hydrostatic strain systems, vacancy and interstitial clustering gradually increased from compression (negative) strain to expansion (positive) strain. However, the slope of negative (compression) uniaxial strain for both vacancy and interstitial clustering was very low. Vacancy clustering increased by approximately 45% and 25% for 2% (positive) hydrostatic and uniaxial strain systems, respectively, as compared with the reference condition with no strain (Figs. 6A and 6B). However, the increase in interstitial clustering was around 55% and 32% for 2% (positive) hydrostatic and uniaxial strain systems, respectively, as compared with the reference condition without applied strain (Figs. 6C and 6D). Hence, positive uniaxial and hydrostatic strain had a larger effect on interstitial clustering than vacancy clustering. In addition to defect-clustered fraction, defect cluster size distribution also impacts radiation damage. Vacancy and interstitial cluster size distributions are presented in Fig. 7 for 20-KeV PKA energy as a function of applied strain type and strain value. Overall, the size of interstitial or vacancy clusters increased under tensile strain for both uniaxial and hydrostatic strains as compared with the reference condition with no applied strain; however, this increase was more linear for hydrostatic strain. The influence of strain on vacancy size was stronger than its effect on the size of interstitials. Positive hydrostatic strain produced the largest vacancy cluster (26 vacancies) (Fig. 7B) and largest interstitial cluster (19 vacancies) (Fig. 7D). Compression strain conditions did not significantly influence the size of vacancy/interstitial clusters. These results indicate that under positive (tensile) strain, defects (vacancy/interstitial) have a greater tendency to agglomerate into larger clusters, which may lead to the formation of voids or dislocation loops [16].

3.3. Temperature effects

The effects of temperature on the number of defects produced by 20-KeV PKA energy under the no-strain, ±2% uniaxial, and ±2% hydrostatic strain conditions are shown in Fig. 8. Strain values as a function of temperature are colored green for no applied strain, pink, red, orange and indigo for +2 % hydrostatic, +2 % uniaxial, -2 % uniaxial and -2 % hydrostatic strain states, respectively. For each strain state, the relationship between the number of Frenkel pairs and temperature was linear, but the slopes of the curves were different. For uniaxial strain, the slope of temperature dependence for the 2% tensile state was slightly greater than that for the 2%

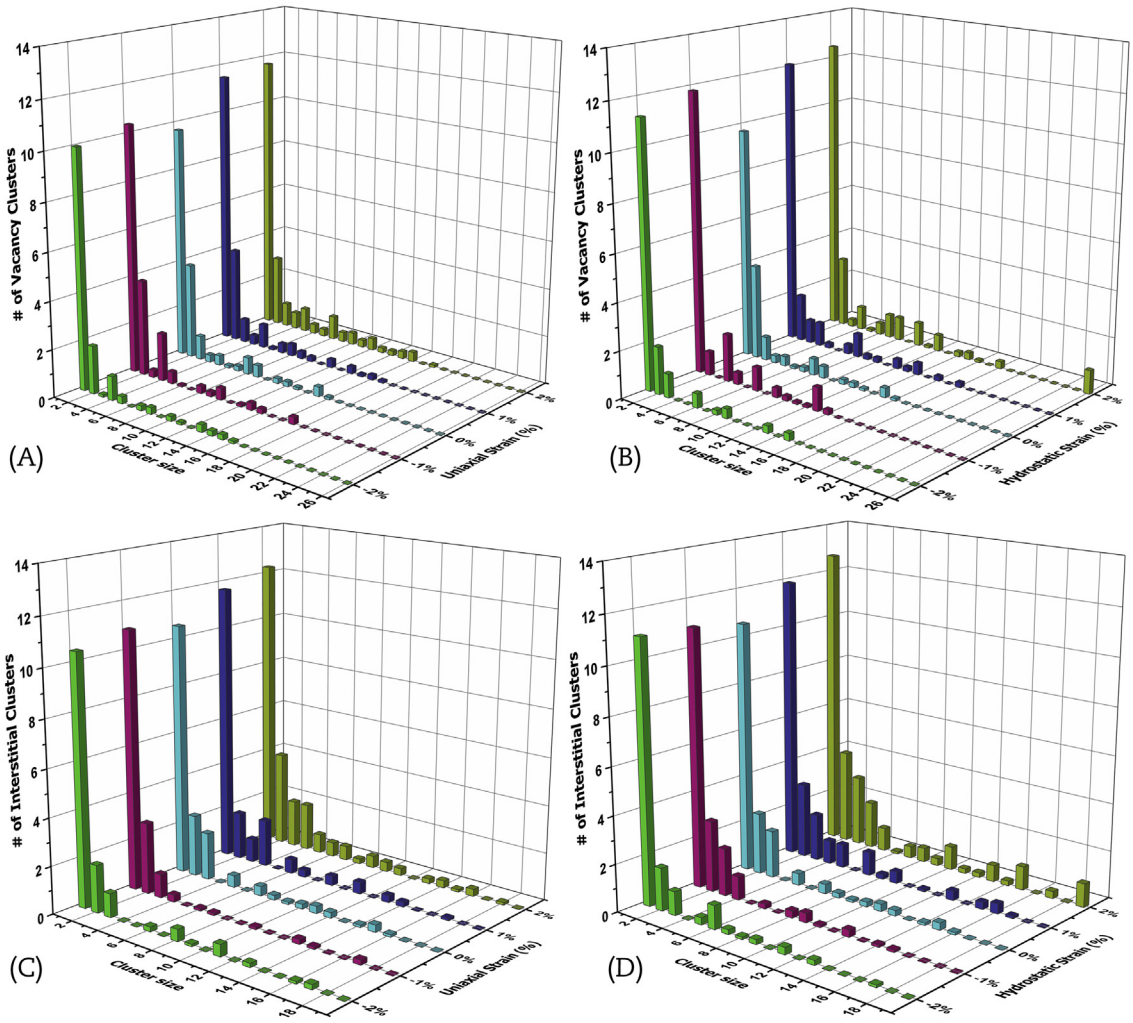

Fig. 7. Vacancies and interstitials cluster size distributions for 20-KeV PKA energy. (A & C) As a function of uniaxial strain. (B & D) As a function of hydrostatic strain. PKA, primary knock-on atom.

compression strain state. However, for the 2% (tensile) hydrostatic state, the slope was much greater than for the −2% (compression) hydrostatic strain condition. These results indicate that hydrostatic strain has a larger influence on the number of Frenkel pairs than no-strain and uniaxial strain states under varying temperature. Although the number of Frenkel pairs decreased with increasing temperature for all strain states due to increased annihilation at higher temperatures, the number of Frenkel pairs produced under tensile strain state was always higher for both uniaxial and hydrostatic strain conditions. These results suggest that the tensile strain

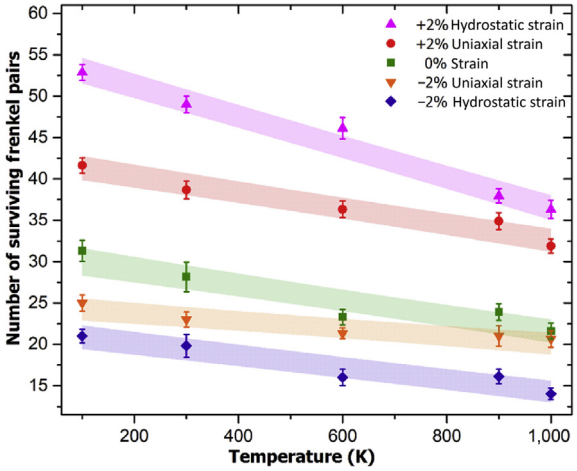

Fig. 8. Temperature dependence of surviving Frenkel pair production for no strain, ±2% uniaxial strain, and ±2% hydrostatic strain systems.

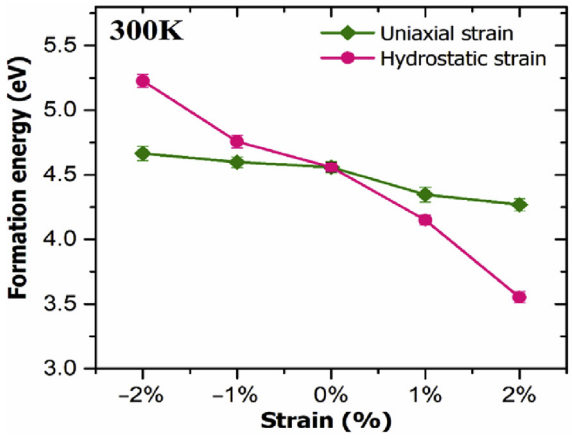

Fig. 9. Strain dependence of Frenkel pair formation energy at 300 K under uniaxial and hydrostatic strain state.

state should be avoided for materials used in a low-temperature radiation environment.

4. Discussion

Based on our observations that strain and temperature influenced the number of generated Frenkel pairs, the number of surviving Frenkel pairs, defect clustering fraction, and the size distribution of defect clusters, we now discuss possible mechanisms underlying these observations. One possible explanation for these results is volumetric changes in response to both uniaxial and hydrostatic strains. Volumetric expansion of the simulation cell influences the production of subcascades, which may affect the generation and annihilation of defects. When an atomic crystal is compressed, its atoms are brought closer to each other. Therefore, the incident energy is dissipated over a smaller volume or creates a smaller displacement cascade region. Moreover, within a compressed crystal, the possibility of atomic movement is also reduced. Therefore, there tend to be fewer displaced atoms because of the presence of additional atoms nearby that restrict atomic movements. However, in the case of tensile/expansion strain, the interatomic distance increases, so the atoms with greater energy move faster and further away from the parent cascade core, making subcascades, thus decreasing the chances of vacancy–interstitial recombination and producing more Frenkel pairs. The number of interstitials produced during cascade processes in a perfect crystal is exactly equal to the number of generated vacancies. Hence, if a certain strain type changes the quantity of one type of defect, it would certainly cause a similar change in the number of other types of defects. Variation in defect formation energies according to the type of strain may be another cause of an increase/decrease in defect production and defect survival. To investigate the effects of strain on defect formation, various systems with and without one Frenkel pair under each strain type and value were simulated at a temperature of 300 K. During the simulation, no interstitial diffusion occurred, and the distance between the vacancy and interstitial clusters was large enough to prevent vacancy–interstitial interactions. Frenkel pair formation energy was calculated as

$$E_{FP} = E_{defect} - E_{Perfect} \quad (2)$$

where E_{defect} is the total energy of the system containing one vacancy/interstitial pair and $E_{perfect}$ is the total energy of the system without defects. Frenkel pair formation energies as a function of strain for both uniaxial and hydrostatic strains are shown in Fig. 9. Frenkel pair formation energy decreased as strain type was varied from compression to tension, and this decrease was very rapid for the hydrostatic strain system. In the uniaxial strain system, the increase in formation energy for compression strain was very slight, which could be why negative (compression) uniaxial strain did not have as great effect on the surviving number of Frenkel pairs (Fig. 4A) as hydrostatic strain. Besides Frenkel pair formation energy, strain and temperature may also have influenced the threshold displacement energy, which could contribute to the results shown in Section 3. The threshold displacement energy decreased from 43.7 and 45.9 eV to 39.2 and 35.6 eV, under uniaxial and hydrostatic strain from −2% (compression) to 2% (tensile), respectively (results not shown).

5. Conclusions

In this study, we carried out MD simulations in α-Zr to investigate the impact of applied strains on the generation of radiation damage at different temperatures. Four PKA energies (1, 5, 10, and 20 KeV), two strain types (uniaxial and hydrostatic), and five strain values ranging from −2% (compression) to 2% (tensile) for each strain type were analyzed. Peak and the stable number of Frenkel pairs (vacancy–interstitial), defect clustered, and their size distribution increased in both uniaxial and hydrostatic strain states from compression (negative) to tensile (positive) strain. However, the effects of hydrostatic strain were more significant than those of uniaxial strain because of a larger volume increase (decrease) which yielded more (less) radiation-induced defects. PKA energy of 20 KeV produced the largest vacancy (26 vacancies) and interstitial (19 interstitials) clusters for 2% hydrostatic strain; however, compression states had no significant impact on the size of the defect clusters. At low temperatures, the applied strains had a larger impact on radiation-induced damage. Overall, the results in the present study suggest that materials used in low-temperature radiation environments should not be exposed to tensile strain.

Conflicts of interest

The authors declare that they have no conflicts of interest.

Acknowledgments

This research was supported by the Nuclear Safety Re-search Program funded by the Nuclear Safety and Security Commission (No. 1305009). The first author highly acknowledged the financial grant provided by the Higher Education Commission (HEC) of Pakistan to support her PhD studies.

Appendix A. Supplementary data

Supplementary data related to this article can be found at https://doi.org/10.1016/j.net.2018.04.013.

References

[1] G.S. Was, Fundamentals of Radiation Materials Science: Metals and Alloys, Springer, 2016.
[2] R. Bullough, B. Eyre, R. Perrin, The growth and stability of voids in irradiated metals, Nucl. Appl. Technol. 9 (1970) 346–355.
[3] S. Chen, B. Liu, L. Lin, G. Jiao, Microstructural development and helium bubble formation in Cu/W (Re) nanometer multilayer films irradiated by He+ ion, Nucl. Instrum. Methods Phys. Res. Sect. B Beam Interact. Mater. Atoms 354 (2015) 244–248.
[4] R. Hengstler-Eger, P. Baldo, L. Beck, J. Dorner, K. Ertl, P. Hoffmann, C. Hugenschmidt, M. Kirk, W. Petry, P. Pikart, Heavy ion irradiation induced dislocation loops in AREVA's M5® alloy, J. Nucl. Mater. 423 (2012) 170–182.
[5] Y. Idrees, Z. Yao, M. Kirk, M. Daymond, In situ study of defect accumulation in zirconium under heavy ion irradiation, J. Nucl. Mater. 433 (2013) 95–107.
[6] C. Chow, R. Holt, C. Woo, C. So, Deformation of zirconium irradiated by 4.4 MeV protons at 347 K, J. Nucl. Mater. 328 (2004) 1–10.
[7] J. Kai, W. Huang, H. Chou, The microstructural evolution of zircaloy-4 subjected to proton irradiation, J. Nucl. Mater. 170 (1990) 193–209.
[8] D.J. Bacon, Y.N. Osetsky, R. Stoller, R.E. Voskoboinikov, MD description of damage production in displacement cascades in copper and α-iron, J. Nucl. Mater. 323 (2003) 152–162.
[9] F. Gao, D. Bacon, L. Howe, C. So, Temperature-dependence of defect creation and clustering by displacement cascades in α-zirconium, J. Nucl. Mater. 294 (2001) 288–298.
[10] R. Voskoboinikov, Y.N. Osetsky, D. Bacon, Identification and morphology of point defect clusters created in displacement cascades in α-zirconium, Nucl. Instrum. Methods Phys. Res. Sect. B Beam Interact. Mater. Atoms 242 (2006) 530–533.
[11] S. Wooding, L. Howe, F. Gao, A. Calder, D. Bacon, A molecular dynamics study of high-energy displacement cascades in α-zirconium, J. Nucl. Mater. 254 (1998) 191–204.
[12] G. Ackland, S. Wooding, D. Bacon, Defect, surface and displacement-threshold properties of α-zirconium simulated with a many-body potential, Philos. Mag. A 71 (1995) 553–565.
[13] N. De Diego, A. Serra, D. Bacon, Y.N. Osetsky, On the structure and mobility of point defect clusters in alpha-zirconium: a comparison for two interatomic potential models, Model. Simulat. Mater. Sci. Eng. 19 (2011) 035003.

[14] H. Khater, D. Bacon, Dislocation core structure and dynamics in two atomic models of α-zirconium, Acta Mater. 58 (2010) 2978–2987.
[15] A. Barrow, A. Korinek, M. Daymond, Evaluating zirconium–zirconium hydride interfacial strains by nano-beam electron diffraction, J. Nucl. Mater. 432 (2013) 366–370.
[16] S. Di, Z. Yao, M.R. Daymond, F. Gao, Molecular dynamics simulations of irradiation cascades in alpha-zirconium under macroscopic strain, Nucl. Instrum. Methods Phys. Res. Sect. B Beam Interact. Mater. Atoms 303 (2013) 95–99.
[17] S. Plimpton, Fast parallel algorithms for short-range molecular dynamics, J. Comput. Phys. 117 (1995) 1–19.
[18] M.I. Mendelev, G.J. Ackland, Development of an interatomic potential for the simulation of phase transformations in zirconium, Phil. Mag. Lett. 87 (2007) 349–359.
[19] C. Domain, Ab initio modelling of defect properties with substitutional and interstitials elements in steels and Zr alloys, J. Nucl. Mater. 351 (2006) 1–19.
[20] C. Domain, A. Legris, Ab initio atomic-scale determination of point-defect structure in hcp zirconium, Philos. Mag. 85 (2005) 569–575.
[21] J. Biersack, J. Ziegler, Refined universal potentials in atomic collisions, Nucl. Instrum. Meth. Phys. Res. 194 (1982) 93–100.
[22] S. Wooding, D. Bacon, A molecular dynamics study of displacement cascades in α-zirconium, Philos. Mag. A 76 (1997) 1033–1051.
[23] P.K. Nandi, J. Eapen, Cascade overlap in hcp zirconium: defect accumulation and microstructure evolution with radiation using molecular dynamics simulations, MRS Online Proc. Libr. Arch. 1514 (2013) 37–42.
[24] ASTM E521-96, Standard Practice for Neutron Radiation Damage Simulation by Charged-particle Irradiation, American Society of Testing and Materials, Philadelphia, PA, 2009.
[25] W. Setyawan, G. Nandipati, K.J. Roche, H.L. Heinisch, B.D. Wirth, R.J. Kurtz, Displacement cascades and defects annealing in tungsten, Part I: defect database from molecular dynamics simulations, J. Nucl. Mater. 462 (2015) 329–337.
[26] N.P. Lazarev, A.S. Bakai, Atomistic simulation of primary damages in Fe, Ni and Zr, J. Supercrit. Fluids 82 (2013) 22–26.
[27] D. Bacon, A. Calder, F. Gao, Defect production due to displacement cascades in metals as revealed by computer simulation, J. Nucl. Mater. 251 (1997) 1–12.
[28] B. Beeler, M. Asta, P. Hosemann, N. Grønbech-Jensen, Effect of strain and temperature on the threshold displacement energy in body-centered cubic iron, J. Nucl. Mater. 474 (2016) 113–119.
[29] J. Guénolé, A. Prakash, E. Bitzek, Influence of intrinsic strain on irradiation induced damage: the role of threshold displacement and surface binding energies, Mater. Des. 111 (2016) 405–413.